Chapter 2

Optical and electrical characteristics of a metal-oxide-semiconductor diode on SiO_2/Si by multi-recipe Si-ion-implantation

2.1 Introduction

Silicon-rich SiO_2 (SiO_x) materials can be synthesized by electron-beam evaporation [1], RF-magnetron sputtering, Si-ion-implantation [2] and plasma-enhanced chemical vapor deposition (PECVD) [3], etc. Si-ion-implantation has recently emerged as an alternative method of synthesizing Si nanocrystals (nc-Si) in SiO_2 matrix. Previously, porous Si [4], PECVD-grown Si-rich SiO_2, amorphous Si:H:O, and Si-implanted SiO_2 ($SiO_2:Si^+$) have been shown to exhibit photoluminescence (PL) and electroluminescence (EL) spreading from blue-green to near infrared region (340-800 nm) region [1, 5-9]. Various defect-related blue-green PL [10-14] bands from $SiO_2:Si^+$ materials have been identified to originate from principle defects such as the neutral oxygen vacancy (NOV, denoted as $O_3\equiv Si-Si\equiv O_3$) with PL at 410-460 nm [15], and the precursor of nc-Si (E'_δ, denoted as Si↑Si–Si) with PL at 520-550 nm [16], the non-bridging oxygen hole center (NBOHC) [15-18], among others. Some of irradiative defects such as NOV and NBOHC can be activated via appropriate annealing processes. The contribution of NOV defects to the PL at 450-470 nm has been verified in previous reports [19-21], whereas the nanocrystallite Si (nc-Si) embedded in the annealed $SiO_2:Si^+$ matrix contributes to the emission at longer wavelengths [11]. The high-temperature annealing of $SiO_2:Si^+$ usually quenches defects and causes the generation of nc-Si, providing a more pronounced near-infrared PL (700-900 nm). The nc-Si related PL wavelength depends strongly on the size of nc-Si. Identifying these irradiative defects

in SiO_2:Si^+ film is very important for white-light emitting applications. The Si-rich SiO_2:Si^+ material with self-assembled Si quantum dots has attracted considerable interest for their potential use in fabricating novel light-emitting or charge-storage devices. Although two contradictory PL mechanisms exist, most studies focus on the nc-Si-correlated PL characteristics, while few studies have investigated the defect-induced blue-green PL.

Time-resolved PL (TRPL) was applied to determine the lifetime and rate of evolution of the concentrations of irradiative defects. Lopez *et al.* reported a lifetime of 55–70 μs for Si dangling-bond centers in SiO_2:Si^+ annealed at 1100 ^oC for 2 h. [23] Amorphous Si exhibited an absorption cross-section of 1×10^{-17} cm^2 and a lifetime of 20 ps, respectively. [24] In particular, Garcia *et al.* characterized the wavelength-dependent TRPL lifetime of SiO_2 with embedded nc-Si, which ranges from 20 to 200 μs as the nc-Si size increases from 2.5 to 7 nm (associated with absorption cross sections from 1×10^{-16} to 1×10^{-15} cm^2). [29] However, few reports have addressed the emission lifetime and concentration of the irradiative defects or their transient luminescent dynamics in SiO_2:Si^+. Pifferi *et al.*[13] investigated the TRPL of thermally annealed SiO_2:Si^+ and determined multiple lifetimes of 0.4, 2 and 10 ns at 450–515 nm, which were explained as the contribution of the E'_{δ} defects that act as precursors of nc-Si. Only defect-dependent TRPL lifetime from 2.3 to 45 ns in oxygen-implanted SiO_2 has been discussed.

In this work, a multi-recipe Si-ion-implantation process is employed to generate a uniformly Si-distributed SiO_2:Si^+ layer on a Si substrate. The luminescent centers in SiO_2:Si^+ before and after thermal annealing are characterized by absorption spectroscopy and electron paramagnetic resonance (EPR). The evolution of defect-enhanced blue-green and white-light PL spectra during different annealing periods is investigated. The defect-enhanced white-light and blue-green EL of a SiO_2:Si^+ metal-oxide-semiconductor (MOS) diode and its corresponding mechanisms are demonstrated. This work also characterizes the category, the concentration and the lifetime of the main irradiative defect in

a multi-recipe $SiO_2:Si^+$ with excess uniformly distributed Si density. The optimized annealing time for the complete activation of defects is evaluated. The lifetimes and the concentrations of irradiative defects at various annealing periods are calculated from the capacitance–voltage (C–V) hysteresis curve and the TRPL plots.

2.2 Material fabrication of Si-ion-implanted SiO_2

The $SiO_2:Si^+$ samples were first prepared by multi-energy Si-ion-implanting the 5000Å-thick SiO_2 film on the (100)-oriented, *n*-type Si substrate with a resistivity of 4-7 Ω-cm. The thickness of the Si substrate was 500 um. The SiO_2 film was deposited by PECVD at a pressure of 400 mTorr using 10 sccm tetraethoxysilane (TEOS) fluence and 200 sccm O_2 fluence at a forward power of 150 W. The Si-implantation conditions were 5×10^{15} ions/cm^2 at 40 keV, 1×10^{16} ions/cm^2 at 80 keV and 2×10^{16} ions/cm^2 at 150 keV. A calculation using a simulating program for "transport of ions in matter code" (TRIM) [5] shows in Fig. 1 that the implantation profile is nearly flat-topped at depths between 100 and 5000 Å below the sample surface. In addition, the secondary ion mass spectrometry (SIMS) of excess Si profile in the $SiO_2:Si^+$ sample is also performed, which is in good agreement with TRIM result (see Fig. 1). After implantation, the samples were encapsulated by annealing at 1100 ^oC in a quartz furnace with flowing N_2 gas for 15 to 300 min, which helped to activate the irradiative defects, to eliminate the carrier-trapping centers and to precipitate Si nanocrystals buried in the SiO_2/Si substrate.

2.3 Experimental setup

After annealing, room-temperature and continuous-wave (CW) PL measurements were performed using a He-Cd laser with a wavelength and average intensity of 325 nm and 5 W/cm^2, respectively, to excite photoelectrons in the $SiO_2:Si^+$ sample. The PL from 360 to

700 nm was detected by a fluorescence spectrophotometer (Jobin Yvon, TRIAX-320) with a wavelength resolution of 0.06 nm using a 1200 g/mm grating, in connection with a cooled photomultiplier (Jobin Yvon, Model 1424M) based on the photon counting technique. The working distance between the focusing lens and the sample was fine-tuned to maximize the PL intensity. A MOS diode was made on the $SiO_2:Si^+$ sample with 2-mm-square, 500 Å-thick silver contacts. After metallization, a sintering process was performed at 150 ^oC for 10 min in the ambient atmosphere. The MOS diode was driven by either a pulsed current source (ILX, LDP-3840) or a voltage source meter (Keithely, 236), using micro-probes (Kar Suss, 253). The scanning ranges of the pulsed current and the CW voltage were from 0 to 3000 mA and from 0 V to 30 V, respectively. The optical power and bias voltage were measured using an optical multi-meter (ILX, 6810B) and a digital multi-meter (Hewlett Packard, HP34401A), respectively. An integrated sphere detector (ILX, OMH-6703B) was employed to collect the light emitted from the surface of the $Ag/SiO_2:Si^+$ /n-Si/Ag MOS diode. The stability of the output power was measured at a pulsed current of 3000 mA for three hours, with period and duty cycle of 10 ms and 10 %, respectively. In the TRPL experiment, the $SiO_2:Si^+$ sample was pumped using a sub-nanosecond flash lamp at a wavelength of 325 nm and a repetition rate of 40 kHz. It was analyzed using a time-correlated single-photon counting system (Edinburgh Instruments, Model FL920) at a wavelength of 410 nm. The lifetime (τ_n) and concentration (N_n) of defects could be determined from the deconvoluted TRPL plot. The C–V analysis of an $Al/SiO_2:Si^+/n$-Si/Al MOS diode with an electrode area of about 1.26×10^{-3} cm^2 was conducted using a C–V meter (Hewlett Packard, 4280A) at a modulation frequency of 1 MHz to verify the concentration of defects in $SiO_2:Si^+$. The hysteresis C-V curve is measured between +15 and -15 V at a stepping rate of 0.05 V/s. The density of hole-trapped defects in $SiO_2:Si^+$ (N_{NOV}) is determined using the equation $N_{NOV} = -\Delta V_{FB} C_{OX} / e$, where C_{ox} is the capacitance of $SiO_2:Si^+$ in the accumulation regime, and ΔV_{FB} is the shift in flat-band voltage obtained from the hysteresis C–V curve of the

$SiO_2:Si^+$ MOS diode.

2.4 Optical properties of the furnace-annealed Si-ion-implanted SiO_2

The PL spectra of $SiO_2:Si^+$ samples before and after annealing at 1100°C from 1 hr to 4 hrs are shown in Fig. 2. After annealing, the PL around 410-460 nm is greatly enhanced, which is never observed from un-implanted SiO_2 and pure Si. Curve-fitting of the broadband PL spectrum reveals three peak wavelengths at 415 nm, 455 nm, and 520 nm with associated linewidths of 35 nm, 52 nm, and 150 nm, respectively. The inset in Fig. 2 presents the PL spectra of the Si substrate, the unimplanted SiO_2/Si, and the implanted $SiO_2:Si^+$/Si samples with and without annealing. As indicated by the inset in Fig. 2, the Si substrate exhibits a relatively weak and broadened PL spectrum between 500 and 550 nm, which becomes much weaker after annealing at 1100 °C for 60 min or longer. Similar results are observed for the unimplanted SiO_2/Si with an even weaker PL intensity before and after annealing at 1100 °C, revealing that very few irradiative defects in the SiO_2/Si contribute to the green PL emission. In contrast, the peak PL intensity of the as-implanted $SiO_2:Si^+$ at 520 nm (in Fig. 2, line a) is equivalent to that of the Si substrate without annealing (Fig. 2 inset, line 1), and is much stronger than that of the SiO_2/Si (Fig. 2 inset, line 3). After annealing, a strong PL peak appears near 410-460 nm, as shown in Fig. 2 (lines b through e). The Si implantation introduces high concentrations of irradiative defects into the SiO_2 film, which were thermally activated to enhance the blue-green PL spectrum at peak wavelengths of 415, 455 and 520 nm with linewidths of 35, 52 and 150 nm, respectively. The origin of these luminescent peaks has been reported [1, 8, 12, 13], but their evolution during long-term annealing has not been extensively addressed. The PL at 415 nm originates from the weak oxygen bond (WOB) defect [5] and the 455 nm luminescence is attributed to the NOV defect.

The NBOHCs emit PL near 600 nm and the origin of the PL at 520 nm is associated with the E'_δ defect. The increase in PL intensity between 410 nm and 455 nm results mainly from the activation of irradiative defects, including WOB and NOV defects in the $SiO_2:Si^+$ film. These structural defects are caused by the physical bombardment of the SiO_2 matrix under a multi-recipe Si-implantation process. Si implantation introduces enormous irradiative defects into the SiO_2 film. The strongest PL peaks at 415-455 nm with linewidths of 35-50 nm are very similar to those obtained by Nishikawa *et al*. [20, 22]. Bae *et al*. [15] have attributed the PL at 455 nm to the transition in the NOV defect [20, 21].

The PL spectra demonstrate that the intensities of the near-infrared PL peaks associated with nc-Si at 820-850 nm are much lower than those from the irradiative defects under all processing conditions. After annealing for 1 hr, the density of NOV defects greatly exceeds that in as-implanted samples. However, the rate of increase in the NOV defect is reduced. A notable stabilization of the defects thermally activated after 2-hr annealing is observed (Fig. 3). However, a longer annealing process (> 4 h) only results in the abrupt decay of both the CWPL intensities and the NOV defect density. As the annealing time is increased to 4 h, the decay of NOV defects is greater than that of other defects - the E'_δ centers with a PL of 520 nm formatted after annealing. The E'_δ center is a small Si cluster that is regarded as a precursor of nc-Si in SiO_2; its PL intensity grows slowly and linearly even following a 4-hr annealing. These results reveal that the promotion in defect-related CWPL is related to the complete activation of NOV defects in the multi-recipe $SiO_2:Si^+$ annealed for up to 3 h, while the optimal annealing temperature and annealing time of 1350°C and 8 h for activating the same defects in $Si:O^+$ are somewhat higher. [8] The observations herein also reveal that defect-related CWPL is initiated much more quickly than nc-Si dependent PL in $SiO_2:Si^+$. The CWPL intensity ratio among as-implanted, 1.5hr-annealed, 3hr-annealed and 4hr-annealed $SiO_2:Si^+$ samples, $P_{as-imp}:P_{1.5-hr}:P_{3-hr}:P_{4-hr}$, is 1 : 20 : 28 : 10, respectively. In contrast, the E'_δ-related PL intensity only doubles after 4-hr annealing.

Figures 3 and 4 plot the evolution of the peak wavelength and the associated intensity, respectively, as functions of the annealing time. The PL intensity abruptly increases within the first 15-min annealing duration due to the rapid elimination of non-radiative defects. The non-radiative defects are eliminated after 60 min. As annealing time more lengthens to 60 min, the activation of NOV defects becomes more pronounced than that of the weak oxygen bond defects, which inevitably leads to a slight red-shift of the PL spectra from 415 nm to 455 nm. The complete activation of these irradiative defects happened after annealing for 90-180 min. The weak oxygen bond defect is initiated after annealing for 45 min, while the density of NOV defects linearly increases. After annealing for more than 90 min, the PL intensity of NOV defects reaches its maximum, while the weak oxygen bond related PL intensity is increasing at a lower rate. Additional energies required for the formation of weak oxygen bond defects from the oxygen interstitials. Although the complete activation of the NOV defect happens earlier than that of the weak oxygen bond defect, the maximum PL intensities of both irradiative defects are within the same order, which corroborates well with the formation mechanism of oxygen vacancies and interstitials in $SiO_2:Si^+$. The concurrent decreasing of NOV and weak oxygen bond related PL intensities are also elucidated. The damaged SiO_2 matrix is gradually regrown as annealing time more lengthens, such a crystallite recovery causes the reversed reactions. That is, the weak oxygen bond breaks up into interstitial oxygen atoms and reacts with the NOV defect and result in a recovery of SiO_2 bond. After annealing for 180 min or longer, the PL intensities at 415 nm and 455 nm decline considerably, whereas the PL intensity at 520 nm tends to remain or slightly grows. It is thus considered that either the dominant irradiative defects change from Si-O species (i.e. weak oxygen bond and NOV defects) to E'_δ or NBOHC defects, or they are annealed out faster than the E'_δ or NBOHC defects at a longer annealing time. Nonetheless, note that high-temperature annealing is expected to produce complete recombination of point defects through the diffusion of mobile oxygen in SiO_2. On the other

hand, such a high-temperature annealing condition (1100 ^{o}C for 15-180 min) has also been employed to precipitate Si nanocrystals in a similar material system in the previous reports. However, the PL spectra of the annealed $SiO_2:Si^+$ samples only show very weak nc-Si-dependent fluorescence at the wavelength range from 700 to 900 nm, which reveals the extremely low density of the nc-Si embedded in the SiO_2. This result follows from the low-dose implantation process, which yields a low Si excess density of <3% in the SiO_2 matrices. In this case, insufficient nc-Si precursors are formed during the annealing process. Hence, it is not contradictory that only blue-green emission (without any distinct sign of red or infrared emission) is observed from our samples.

The displacement of oxygen from a normal SiO_2 site generates neutral oxygen vacancies instead of dense Si interstitials, which remain in SiO_2 following Si implantation, [11,12] and the oxygen interstitials (the precursors for the weak oxygen bond defects) are generated concurrently. The NOV is configured by two threefold-coordinated silicon atoms bound to the other fragment of the SiO_2 network, where two silicon atoms form a weak Si–Si bond. [10] This can be described by the reaction rule of $O_3\equiv Si\text{-}O\text{-}Si\equiv O_3 \rightarrow O_3\equiv Si - Si\equiv O_3 + O_{interstitial}$. The Si implantation not only induces strong displacement of the oxygen bonds but also generates enormous silicon/oxygen interstitials from the damaged lattice. Weak oxygen bond defects transfer from the oxygen interstitials after longer annealing, which is expressed by the reaction of $O_{interstitial} + O_{interstitial} \rightarrow O - O$. The E'_{δ} center contributes to the emission at 520 nm, which is basically a SiO_4 vacancy substituted by a single four-valent Si atom. [11] In addition, a red shift of nc-Si dependent PL from 826 nm to 856.5 nm with its maximum intensity after 3-hr annealing is also observed, however, which are much weaker than those from the irradiative defects. It reveals that the present implanting dosage is insufficient to help precipitate high-density nc-Si, giving rise to a lower intensity than that attributed by the irradiative defects.

Such a strong blue-green emission is caused mainly by the activation of dense

irradiative NOV defects in $SiO_2:Si^+$, which is generated by physically bombarding the SiO_2 using such as the ion-implanting process. The luminescence in this band is thus attributed to the transition between the ground state (singlet) and the elevated state (triplet) of the NOV defect. [6, 11] The PL intensity is increased by more than one order of magnitude, because of the full activation of the NOV defects during 3hr annealing. The strongest PL peaks at 410–460 nm with a linewidth of 35–50 nm are very similar to those obtained by Nishikawa *et al.* [20] Similar results were also obtained from the Si-implanted SiO_2 grown by thermal oxidation (2–3×10^{17} cm^{-2}, 80–190 keV), [2] Ge-implanted SiO_2 (5×10^{15} cm^{-2}, 80 keV) [6] and Ir^{2+}-implanted silica glass (0.6–7×10^{16} cm^{-2} , 2 MeV). [13] However, these PL peaks were rarely obtained from other Si-rich SiO_2 samples prepared without applying ion-implantation methods.

The formation of both paramagnetic E' centers ($O_3{\equiv}Si{\cdot}^{+}Si{\equiv}O_3$) and diamagnetic NOV ($O_3{\equiv}Si{-}Si{\equiv}O_3$) defects has also been observed in most ion-implanted or radiation-damaged SiO_2. The oxygen vacancy is the precursor to the formation of the E' center, [14] while a hole trapped at the site of the oxygen vacancy forms the E' center (a positively charged oxygen vacancy).[15,16] That is, $O_3{\equiv}Si{-}Si{\equiv}O_3 + h^+ \rightarrow O_3{\equiv}Si{\cdot}^{+}Si{\equiv}O_3$, where h^+ denotes the trapped hole state. Hole trapping yields a positively charged NOV defect ($O_3{\equiv}Si{\cdot}^{+}Si{\equiv}O_3$), or the E' center in $SiO_2:Si^+$ can induce a space charge effect, which inevitably leads to the clear hysteresis in the C–V response of a MOS diode made on $SiO_2:Si^+$ (see Fig. 5). For example, the as-implanted $SiO_2:Si^+$ exhibits a flat-band voltage shift (ΔV_{FB}) of -0.89 V corresponding to a NOV defect concentration of 8×10^{16} cm^{-3}. Fitting the TRPL plots shown in Fig. 6 demonstrates that the lifetime of the NOV defects is shortened from 25.9 to 3.6 ns as the annealing time is increased to 3 h. As the annealing time is increased further to 4 h, the TRPL lifetime is slightly lengthened to 5.1 ns. The TRPL lifetime of the E'_δ centers decreases (from 47.5 to 23 ns) more slowly with annealing time. This result is consistent with the slow formation of E'_δ centers (the nc-Si precursor) in $SiO_2:Si^+$. The slowly varied

lifetime and concentration of E'$_\delta$ defects also indicate that the excess density of Si does not suffice for the efficient precipitation of dense nc-Si in the SiO_2 matrix. The origins of these luminescent peaks have been reported, [1,8,12,13] but their enhancement during long-term annealing has never been addressed. The 415 nm PL emission originates from the weak oxygen bond defect [5] and the 455 nm (2.7 eV) luminescence is attributed to the NOV defect. The NBOHCs yields emission near 600 nm. Additionally, the origin of the 520 nm PL emission is associated with the E'$_\delta$ defect. The EPR measurement was made to prove the existence of E'$_\delta$ defects, which reveals the complete activation of E'$_\delta$ defects in annealed SiO_2:Si^+ for 180 min. (see Fig. 7). [25,26] The corresponding zero-crossing g value for the E'$_\delta$ defect is approximately 2.0019, which coincides well with previous reports. [27,28]

Figure 8 plots the carrier lifetimes and corresponding concentrations of NOV and E'$_\delta$ defects as a function of annealing time. The lifetime ratio of the NOV (τ_{NOV}) in as-implanted, 1.5hr-implanted, 3hr-annealed and 4hr-annealed SiO_2:Si^+ samples, $\tau_{as\text{-}imp}$: $\tau_{1.5\text{-}hr}$: $\tau_{3\text{-}hr}$: $\tau_{4\text{-}hr}$, is about 1: 0.16: 0.14: 0.2. According to the absorption cross section of the NOV defects of σ_{NOV} = 8 $\times10^{-17}$ cm^2 estimated by Nishikawa *et al.* [27], the NOV defect concentration of SiO_2:Si^+ annealed for 3 h has increased from 2.5×10^{16} to 4.8×10^{17} cm^{-3}. The difference between the calculated NOV defect concentrations obtained by C–V and TRPL analyses is less than one order of magnitude. The absorption cross section (~1×10^{-17} cm^{-2}) extrapolated from the experimental data presented by Garcia *et al.* [29] reveals that the E'$_\delta$ defect concentration increases from 1.3×10^{17} to 2.6×10^{17} cm^{-3} (as determined by TRPL analysis). The calculated lifetimes of the E'$_\delta$ defect of size <0.8 nm, ranging from 23–47.5 ns, are much smaller than all those reported for large-scale nc-Si (> 2.5 nm). Four hours of annealing reduced the density of NOV defects to 1.7×10^{17} cm^{-3}, but left whereas the concentrations of the E'$_\delta$ defects at 2.7×10^{17} cm^{-3}.

2.5 Electrical properties of the furnace-annealed Si-ion-implanted SiO_2

Figure 9 presents the measured CW and pulsed current-voltage (I-V) characteristics of the Ag/SiO_2:Si^+/n-Si/Ag MOS diode. The turn-on voltage of the MOS diode under the pulsed driving condition is 5.8 V, which is much smaller than that of the Ag/SiO_2/n-Si/Al MOS diode reported previously [30]. The CW I-V measurements of the Ag/SiO_2:Si^+/n-Si/Ag MOS diode further reveal a negative-differential-resistance effect with a comparable threshold field strength (300 kV/cm) to that of the GaN semiconductors (80-150 kV/cm) [31,32]. The resistance of the Ag/SiO_2:Si^+/n-Si/Ag MOS diode is about 7.9 ohms at a bias voltage between 0 V and 9 V, but the resistance decreases to 0.6 ohms after turn-on. Significantly, the turn-on voltage of the Ag/SiO_2:Si^+/n-Si/Ag MOS diode is almost one order of magnitude lower than that of an Ag/SiO_2/n-Si/Al diode (up to 50 V) reported by Yuan *et al.* [30]. Under pulsed current driving conditions, the optical power of the SiO_2:Si^+ MOS diode driven from 0 A to 3 A is shown in Fig. 10. Extrapolating the output optical power as a function of the bias current or voltage reveals that the threshold current of the Ag/SiO_2:Si^+/n-Si/Ag MOS light emitting diode is 0.28 A. Such a low turn-on voltage of the emission of light from the Ag/SiO_2:Si^+/n-Si/Ag MOS diode SiO_2:Si^+ sample with a SiO_2:Si^+ thickness of 500 nm is mainly attributed to the improvement (modification) of the carrier transport of the Ag/SiO_2:Si^+/Si/Ag MOS diode, which is strongly related to the enhanced Fowler-Nordheim tunneling behavior induced after the multi-energy Si-implantation process. The optical power increases by nearly four orders of magnitude as the drive current is increased from 0.28 A to 0.97 A. The maximum optical power is about 120 nW at a bias current of 0.97 A. By measuring a single luminescent point of the Ag/SiO_2:Si^+/n-Si/Ag diode with a lensed fiber, the power-current (P-I) slope is determined as to be 1.56×10^{-5} mW/A. Note that such a small slope is due to the measuring limit of the power sensor. The

optical power at a constant drive current is relatively stable, with a fluctuation of less than 5%. As the drive current exceeds 1 A, the output power tends to saturate due to the finite density of minority carrier (holes) in n-Si injected into the $SiO_2:Si^+$ layer (see Fig. 10).

The EL wavelength of the $Ag/SiO_2:Si^+$/n-Si/Ag MOS diode is completely different from that of an Ag/SiO_2/n-Si/Al diode (with red luminescence at wavelengths of 620-640 nm) [10]. In particular, the EL pictures of the $Ag/SiO_2:Si^+$/n-Si/Ag MOS diode biased at various pulsed-currents (see Fig. 13) reveal different colors under different bias conditions. The deep-blue EL is more pronounced at a bias current near threshold, which turns into the white-light luminescence at a bias current of 1.25 A. However, the dominant EL wavelength further increases into the green region as the bias current becomes extremely high (>2 A). At a bias current of 0.35 A, the deep-blue EL spectrum (see Fig. 14) of the MOS diode is between 400 and 450 nm since the recombination by WOB defects is preferable under near-threshold condition. The white-light EL spectrum of the MOS diode at a bias current of 1.25 A is between 400 and 600 nm, while the green EL spectrum at 3 A is between 450 and 550 nm. At a bias current of 1.25 A, the white-light emission is attributed to a full recombination through three different centers, including the WOB defects (~415 nm), the NOV defects, and the E'_δ defects (~520 nm). At a high bias current (> 2 A), the green-region spectrum is clearly enhanced due to the highest density of NOV defects in $SiO_2:Si^+$. The EL intensity at a bias current of 3 A is six times higher than that at 0.35 A. Additionally, the emission spot becomes larger at a higher bias. The lifetime testing of such an EL emitting diode is performed by measuring its time-dependent power characteristic, as shown in the inset of Fig. 12. Under a pulsed bias of 3 A, the decay in output power of the $Ag/SiO_2:Si^+$/n-Si/Ag MOS diode under TEC cooling is up to 58% within 3 hrs.

The EL spectrum of the $Ag/SiO_2:Si^+$/n-Si/Ag MOS diode deviates slightly from that of the PL, which originates from an impact ionization and subsequent electron-hole recombination under a high electric field. Previously, Heikkilä *et al.* [33] have studied

versatile carrier transport mechanisms of the metal/SiO_2/p-Si/metal diode. The light emission from such a MOS diode is mainly dependent on the defects near the interface of the SiO_2/p-Si, which exhibits EL at both the forward and reverse bias conditions only when the contact metal is ohmic-like. The schematic energy band diagrams of the metal/SiO_2/p-Si/metal structure under forward and reverse bias are shown in the previous work [19, 30, 33]. If a forward bias is sufficiently large, most electrons from the negatively biased metal contact can tunnel through the SiO_2 into the conduction band of p-Si substrate and some electrons can be trapped by the higher energy levels of the defects in the SiO_2 [19, 33]. The holes (majority carriers) in p-Si can also be injected into the SiO_2 and be trapped by higher energy levels of the defects in the SiO_2. The irradiative recombination of charged carriers at these occupied defect states in the SiO_2 is responsible for the visible EL. When the metal/SiO_2/p-Si/metal diode is negatively biased, the holes can hardly be supported by the metal contact and the electrons are the minority carriers in p-Si. Consequently, a strong EL is rather difficult unless the MOS diode is strongly reverse-biased.

In addition, Yuan *et al.* [30] also observed a visible EL at 620-640 nm from a reverse biased Ag/native-SiO_2/n-Si/Al (referred to as Ag/SiO_2/n-Si/Al) diode, which results from the recombination of NBOHC centers near the SiO_2/n-Si interface. The carrier injection of such a diode structure relies on the field-dependent impact ionization [19, 30, 33]. Under a reverse bias, an inversion layer can be formed just beneath the SiO_2/n-Si interface, which accumulates the minority carriers (holes) in n-Si as shown in Fig. 5(b) of Ref. 30. The tunneling electrons from the metal contact and holes from the n-Si are subsequently trapped and radiatively recombine through the NBOHC states. In particular, a forward bias fails to induce EL since it is difficult to inject hole from the positively biased metal contact. These observations correlate well with previous reports where the metal contact must supply electrons rather than holes. Such polarization dependence also excludes the possibility of EL from nc-Si (if it exists) within the SiO_2. Later on, Bae *et al*. [15] stated that the EL observed

in a Au/SiO_x/p-Si/metal diode under reverse bias is attributed to the impact ionization of the ground state electrons of the NOV centers in SiO_x. It is considered that luminescent efficiency by direct tunneling under a forward bias is less pronounced than that by impact ionization under reverse bias, although the direct tunneling helps the transport of carriers under forward bias conditions.

In comparison, our experimental results are somewhat similar to those reported previously [22, 10], which reveals that the EL of the Si-rich $SiO_2:Si^+$ layer decreases under forward-bias conditions [19, 34, 35]. The EL can only be obtained when the Ag/$SiO_2:Si^+$/n-Si/Ag diode is reverse biased in our case, which is enhanced by stronger impact ionization on the ground states of defects via the accumulation of injected holes in the inversion layer formed beneath the $SiO_2:Si^+$/n-Si interface. In general, multi-energy Si-ion-implantation introduces high densities of various defects that are uniformly distributed in the thin $SiO_2:Si^+$ layer. With increasing bias, the tunneling electrons and holes can be trapped and subsequently recombine in the occupied WOB defect, NOV defects, and E'_δ defects. A higher electric field increases the band bending in the accumulation layer, which facilitates the tunneling of holes from the n-Si substrate to the ground states of NOV and E'_δ defects (See Fig. 15). Such an operation greatly enhances the transitions contributing to the blue-yellow luminescence. Both the transitions contributed by the WOB defects and NOV defects can emit the deep-blue luminescence at lower bias currents. The white-light EL emission is observed when the bias current increases before the saturation of output power. The green EL from the E'_δ will be enhanced when the bias current (as well as the electric field) becomes extremely high. The reason for the saturated output-power at a bias current of nearly 1 A is due to the limited density of the minority carriers (holes) in the n-Si substrate. A stronger bias seriously bends the inversion layer beneath the $SiO_2:Si^+$/n-Si interface and thus greatly accumulates the holes at lower states, which subsequently tunnel into the E'_δ defects at higher energy levels (see Fig. 15). This effect results in longer luminescent

wavelengths at higher bias conditions. Nonetheless, such an impact ionization process usually requires a strong bias, which inevitably causes the substrate to overheat.

2.6 Conclusion

In conclusion, the white-light and blue-green EL from an Ag/SiO_2:Si^+/n-Si/Ag MOS diode with the defect-enhanced blue-green PL, made on a thermally annealed, multi-recipe Si-ion-implanted SiO_2:Si^+ film on a Si substrate with a nearly depth-independent Si-dose distribution profile, are studied. After annealing for 180 min, the main irradiative defects corresponding to PL at 415, 455 and 520 nm are completely activated. These defects are identified as WOB, the NOV-related defects and E'_δ-related defects, respectively. The annealing time is optimized to 3 h to activate completely the NOV defects and enhance the PL intensity. The ion-implantation introduces more dangling bond defects than other methods (such as PECVD and sputtering) for synthesizing the Si-rich SiO_2. During the Si implantation (or physical bombardment with high-energy ions), the oxygen vacancies and the oxygen interstitials (the precursors for the WOB defects) are created due to the relatively large quantities of oxygen that are displaced from their atomic positions in the SiO_2 matrix. In comparison with NOV defects, additional energy is required to form WOB defects from the oxygen interstitials. The NOV defects are therefore activated faster than the WOB defects for a given annealing condition, however, the increase in the number of both NOV and WOB radiative defects are of the same order of magnitude. This result again confirms the reaction rule for oxygen vacancies and interstitials in SiO_2:Si^+. A longer annealing eliminates a significant number of NOV defects, but the slow increase in the density of the E'_δ defects persists. The NOV defect concentration is found to rise from 2.5×10^{16} to 4.8×10^{17} cm^{-3} during 3-hr annealing; the data obtained from the C–V analysis agree quite well with those obtained by TRPL analysis, which also reveals a reduction in the luminescent lifetime from

26 to 3.6 ns. This result is consistent with the CWPL results, which reveal that 3-hr annealing increases the intensity by one order of magnitude. In contrast, the decreasing in the lifetime of the E'$_{\delta}$-defect-dependent TRPL is moderate (from 47.5 to 23 ns). The reduction in the density of the WOB defects is more pronounced than that of NOV defects since two oxygen interstitials are required to generate a WOB defect. The complete activation of the E'$_{\delta}$ defects does not happen in experimental results, which reveals the nc-Si structures have not yet been well constructed. The EL power of the Ag/SiO_2:Si^+/n-Si/Ag MOS diode increases linearly with bias current after turn-on, and saturates near 0.97 A. The EL of the Ag/SiO_2:Si^+/n-Si/Ag MOS diode turns from blue to white-light emission when the bias current is close to the saturation condition, and eventually changes to a yellow-green emission as the bias current is increased to 3 A. The EL spectrum of the MOS diode under different reverse bias conditions indicates that the irradiative recombination is due to enhanced impact ionization of ground states of defects, such as WOB, NOV, and E'$_{\delta}$ defects, through the injection of holes accumulated in the inversion layer formed beneath the SiO_2:Si^+/n-Si interface.

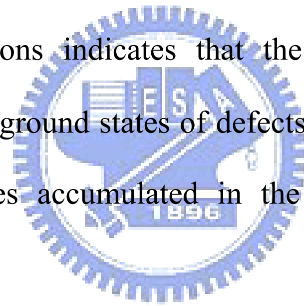

References

[1] Q. Ye, R. Tsu, and E. H. Nicollian, Phys. Rev. B **44**, 1806 (1991).

[2] A. Pèrez-Rodrìguez, O. González-Varona, B. Garrido, P. Pellegrino, J. R. Morante, C. Bonafos, M. Carrada, and A. Claverie, J. Appl. Phys. **94**, 254 (2003).

[3] D. Pacifici, E. C. Moreira, G. Franzo, V. Martorino, and F. Priolo, Phys. Rev. B **65**, 144109-1 (2002).

[4] L. T. Canham, Appl. Phys. Lett. 57, 1046 (1990).

[5] X. Zhao, O. Schoenfeld, J. Kusano, Y. Aoyagi, and T. Sugano, Jpn. J. Appl. Phys. **33**, L899 (1994).

[6] P. Mutti, G. Ghislotti, S. Bertoni, L. Bonoldi, G. F. Cerofolini, L. Meda, E. Grilli, and M. Guzzi, Appl. Phys. Lett. **66**, 851 (1995).

[7] T. Shimizu-Iwayama, K. Fujita, S. Nakao, K. Saitoh, T. Fujita, and N. Itoh, J. Appl. Phys. **75**, 7779 (1994).

[8] H. Takagi, H. Owada, Y. Yamazaki, A. Ishizaki, and T. Nakagiri, Appl. Phys. Lett. **56**, 2379 (1990).

[9] S. Tong, X. N. Liu, T. Gao, and X. M. Bao, Appl. Phys. Lett. **71**, 698 (1997).

[10] L. S. Liao, X. M. Bao, X. Q. Zhen, N. S. Li, and N. B. Min, Appl. Phys. Lett. **68**, 850 (1996).

[11] S. Guha, J. Appl. Phys. **84**, 5210 (1998).

[12] S. T. Chou, J. H. Tsai, and B. C. Sheu, J. Appl. Phys. **83**, 5394 (1998).

[13] A. Pifferi, P. Taroni, A. Torricelli, G. Valentini, P. Mutti, G. Ghislotti, and L. Zanghieri, Appl. Phys. Lett. **70**, 348 (1997).

[14] C. Barthou, P. H. Duong, A. Oliver, J. C. Cheang-Wong, L. Rodriguez-Fernandez, A. Crespo-Sosa, T. Itoh, and P. Lavallar, J. Appl. Phys. **93**, 10110 (2003).

[15] H. S. Bae, T. G. Kim, C. N. Whang, S. Im, J, S. Yun, and J. H. Song, J. Appl. Phys. **91**,

4078 (2002).

[16] H. Z. Song and X. M. Bao, Phys. Rev. B **55,** 6988 (1997).

[17] G. G. Qin, A. P. Li, B. R. Zhang, and B. C. Li, J. Appl. Phys. **78**, 2006 (1995).

[18] F. J. Feigl, W. B. Fowler, and K. L. Yip, Solid State Commun. **14**, 225 (1974).

[19] W. Hayes, M. J. Kane, O. Salminen, R. L. Wood, and S. P. Doherty, J. Phys. C: Solid State Phys. **17**, 2943 (1984).

[20] H. Nishikawa, E. Watanabe, D. Ito, M. Takiyama, A. Leki, and Y. Ohki, J. Appl. Phys., **78**, 842 (1995).

[21] R. Tohmon, Y. Shimogaichi, H. Mizuno, Y. Ohki, K. Nagasawa, and Y. Hama, Phys. Rev. Lett. **62**, 1388 (1989).

[22] H. Nishikawa, R. Nakamura, and J. H. Stathis, Phys. Rev. B **60**, 15910 (1999).

[23] M. Lopez, B. Garrido, C. Garcia, P. Pellegrino, A. Perez-Rodriguez, J. R. Morante, C. Bonafos, M. Carrada, and A. Claverie, Appl. Phys. Lett. **80**, 1637 (2002.)

[24] J. Kudrna, P. Maly, F. Trojanek, I. Pelant, J. Kocka, A. Poruba, S. Surendran, and J. Jiricka, J. Lumin. **80**, 435 (1999).

[25] K. Vanheusden and A. Stesmans, J. Appl. Phys. **74**, 275 (1993).

[26] Y. Sakurai and K. Nagasawa, J. Appl. Phys. **86**, 1377 (1999).

[27] H. Nishikawa, E. Watanabe, D. Ito, Y. Sakurai, K. Nagasawa, and Y. Ohki, J. Appl. Phys. **80**, 3513 (1996).

[28] M. Ya. Valakh, V. A. Yukhimchuk, V. Ya. Bratus, A. A. Konchits, P. L. F. Hemment, and T. Komoda, J. Appl. Phys. **85**, 168 (1999).

[29] C. Garcia, B. Garrido, P. Pellegrino, R. Ferre, J. A. Moreno, J. R. Morante, L. Pavesi, and M. Cazzanelli, Appl. Phys. Lett. **82**, 1595 (2003).

[30] J. Yuan and D. Haneman, J. Appl. Phys. 86, 2358 (1999).

[31] G.-R. Lin, Jpn. J. Appl. Phys. **41**, L1379 (2002).

[32] E. Alekseer and D. Pavlidis, Solid-State Electron. **44**, 941 (2000).

[33] L. Heikkilä, T. Kuusela, and H.-P. Hedman, J. Appl. Phys. **89**, 2179 (2001).

[34] M. Kimura and H. Koyama, J. Appl. Phys. **85**, 7671 (1999).

[35] H. J. Wen and R. Ludeke, J. Vac. Sci. Technol. B **15**, 1080 (1997).

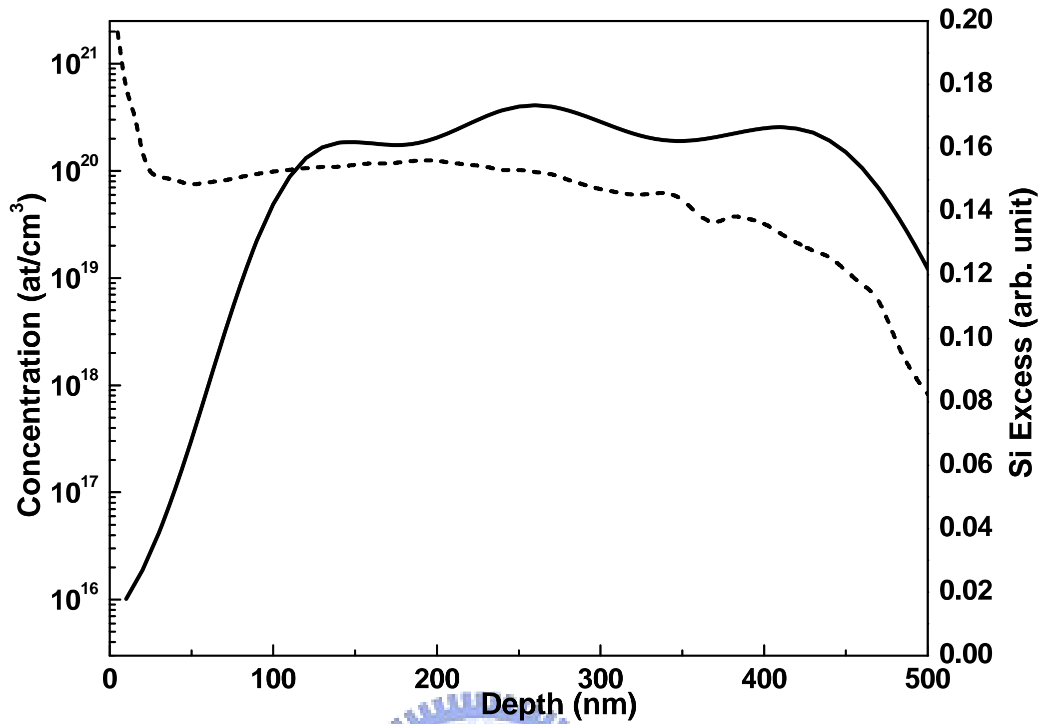

Fig. 1 The secondary ion mass spectrometry result and the TRIM-calculated excess Si-atom density in multi-energy Si-ion-implanted $SiO_2:Si^+$ sample as a function of implanting depth.

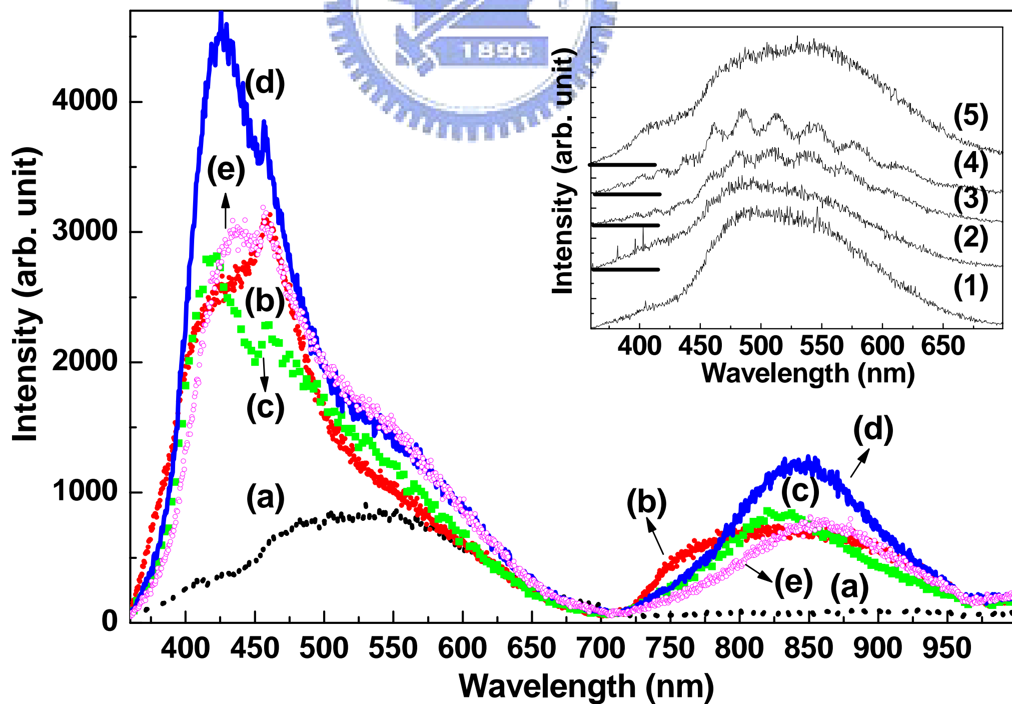

Fig. 2 PL spectra of the $SiO_2:Si^+/Si$ samples at (a) as-implanted condition, or annealed at 1100 °C for (b) 30, (c) 60, (d) 180 and (e) 240 min. The inset figure plots the PL spectra of (1) n-type Si substrate (2) 60-min annealed n-type Si substrate (3) SiO_2/Si sample (4) 60-min annealed SiO_2/Si sample and (5) as-implanted substrate.

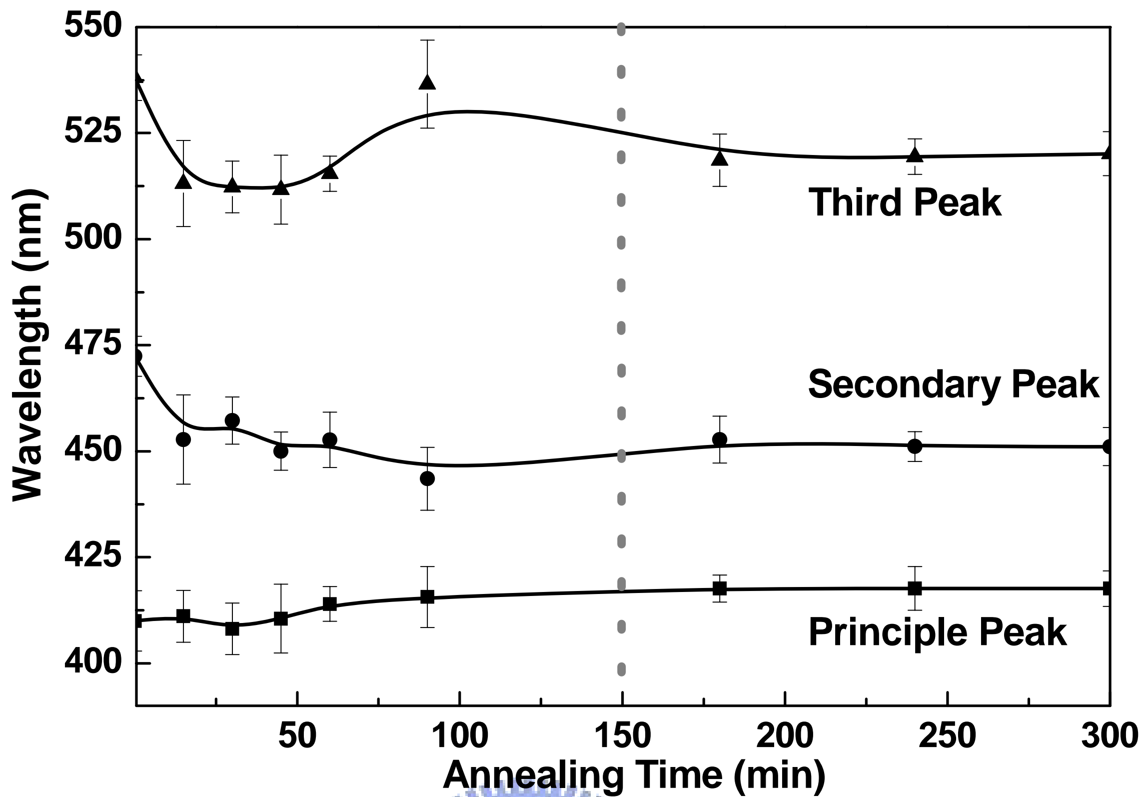

Fig. 3 Wavelength evolution of three PL peaks in SiO_2:Si^+ samples as-implanted or annealed at 1100 °C for different annealing times.

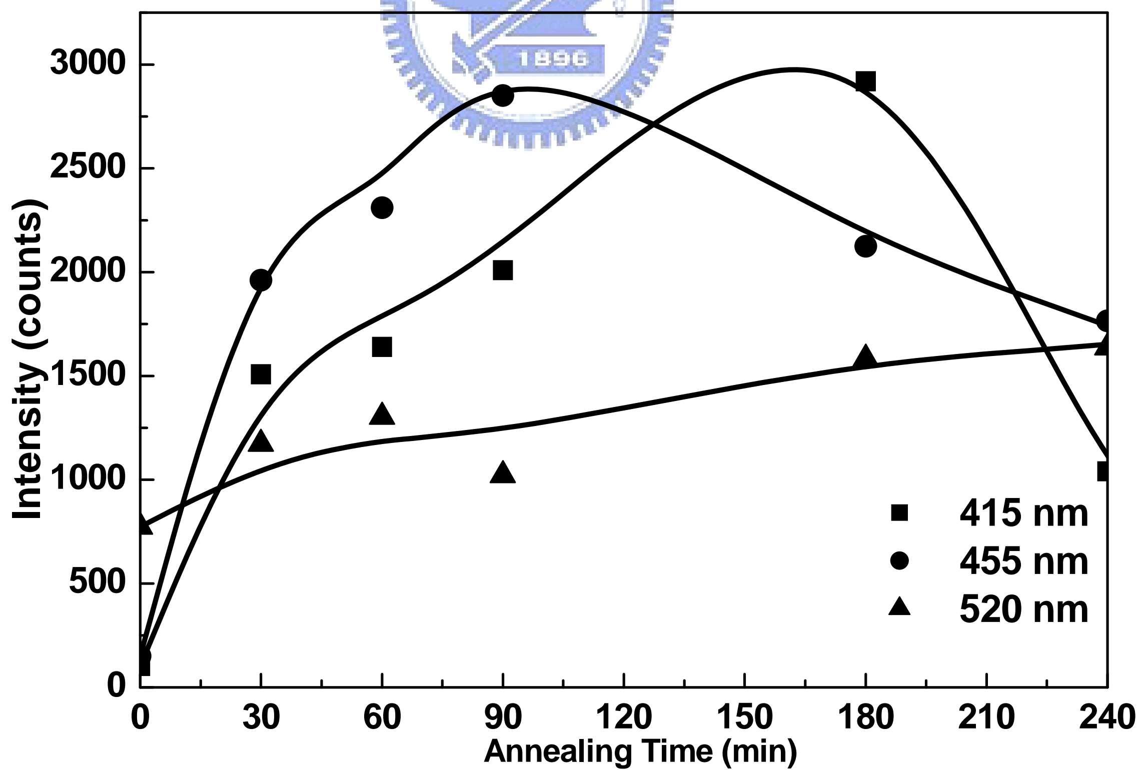

Fig. 4 The annealing-time dependent PL intensities at different wavelengths of 415 nm, 455 nm, and 520 nm.

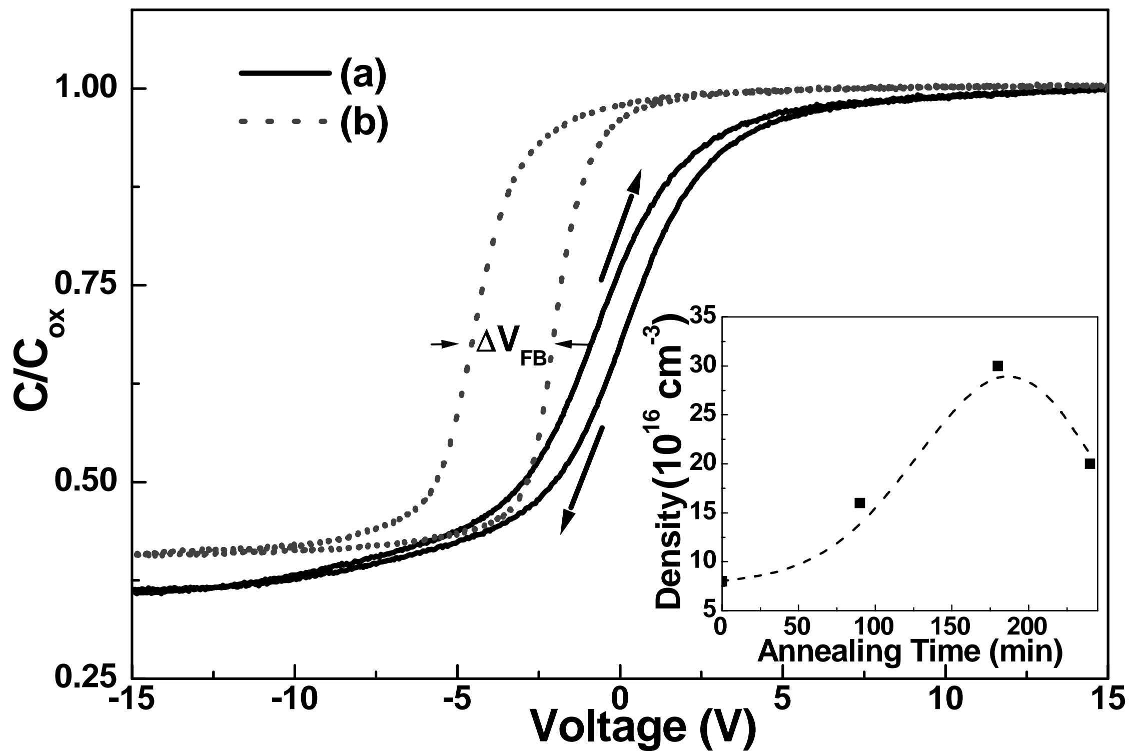

Fig. 5 C–V hysteresis measurement of MOS diode made on (a) as-implanted $SiO_2:Si^+$ and (b) $SiO_2:Si^+$ annealed at 1100 ^oC for 3 h. The inset figure shows the NOV defect concentration as a function of annealing time obtained from C–V analysis.

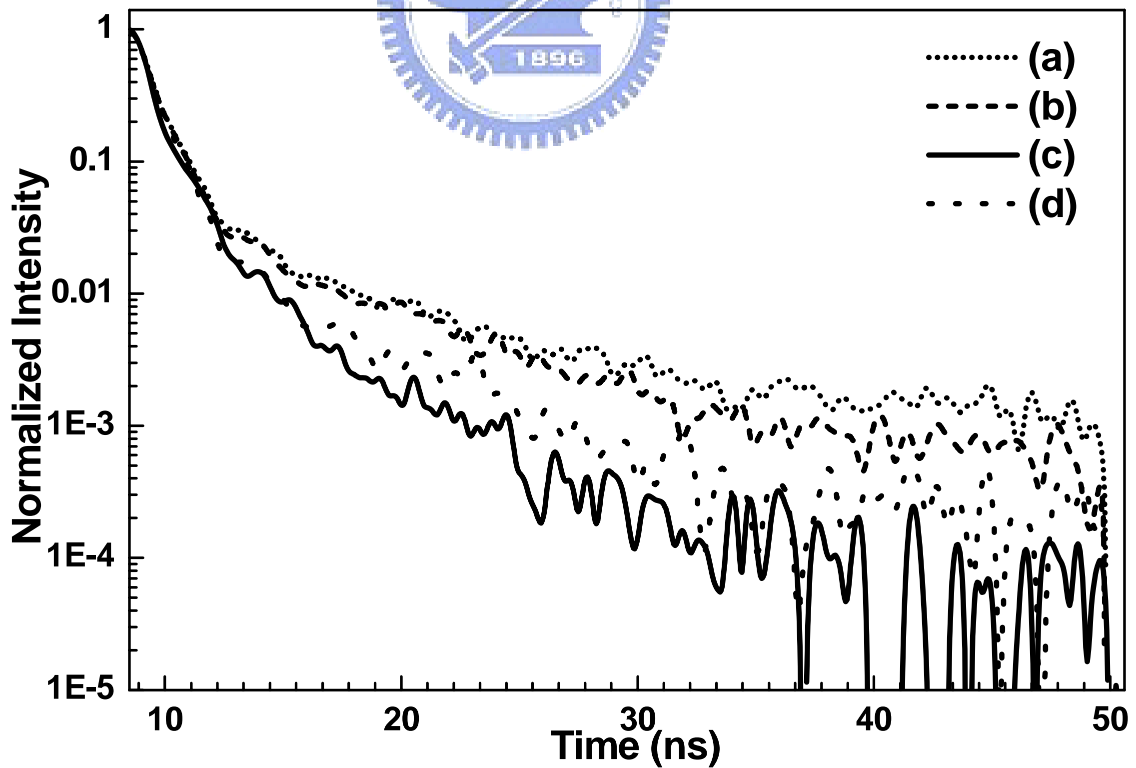

Fig. 6 Normalized TRPL spectra of $SiO_2:Si^+$ samples at (a) as-implanted condition, or annealed at 1100 ^oC for (b) 1.5 h, (c) 3 h and (d) 4 h.

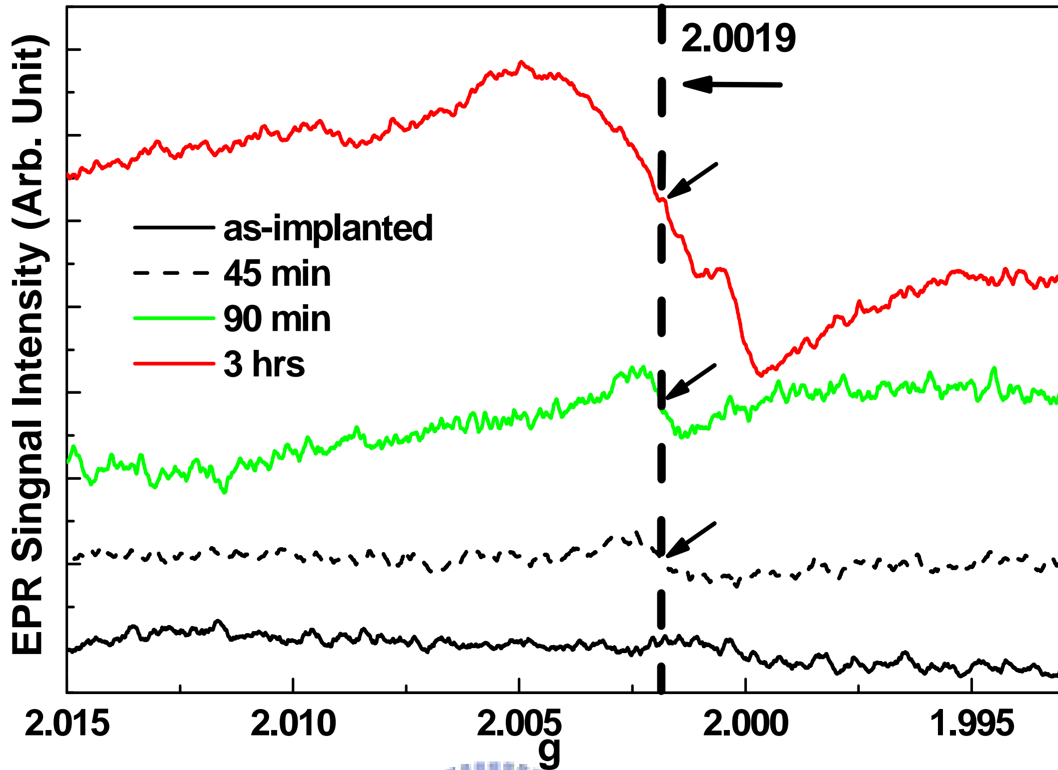

Fig. 7 EPR spectra of the $SiO_2:Si^+$ samples at as-implanted condition, and annealed at 1100 °C for 45, 90 and 180 min.

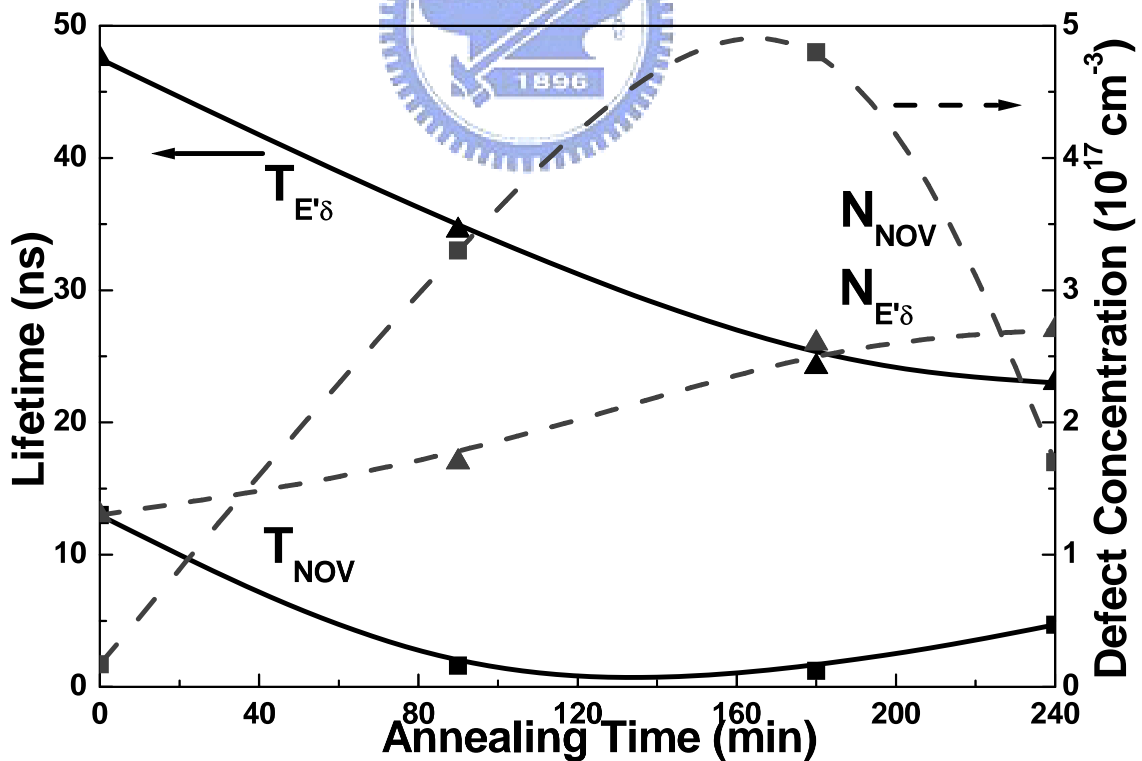

Fig. 8 TRPL lifetime and concentrations of NOV and E'_{δ} defects in $SiO_2:Si^+$ at different annealing times.

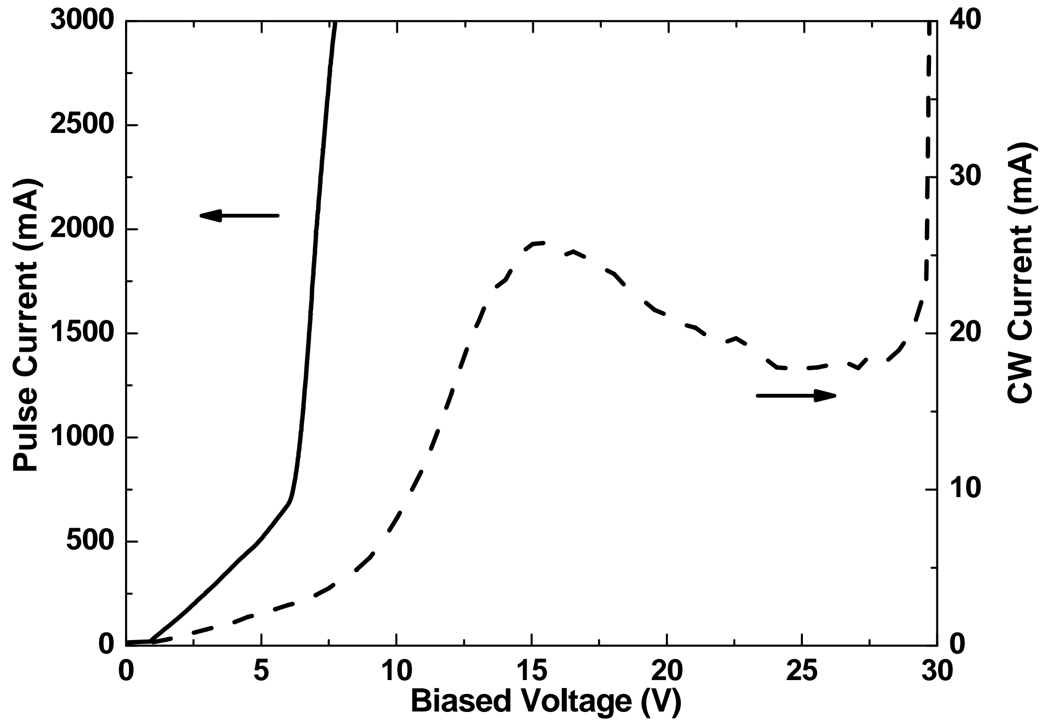

Fig. 9 CW and pulsed current-voltage measurements of $Ag/SiO_2:Si^+/n$-Si/Ag MOS diode with $SiO_2:Si^+$ annealing at 1100 ^oC for 180 min.

1896

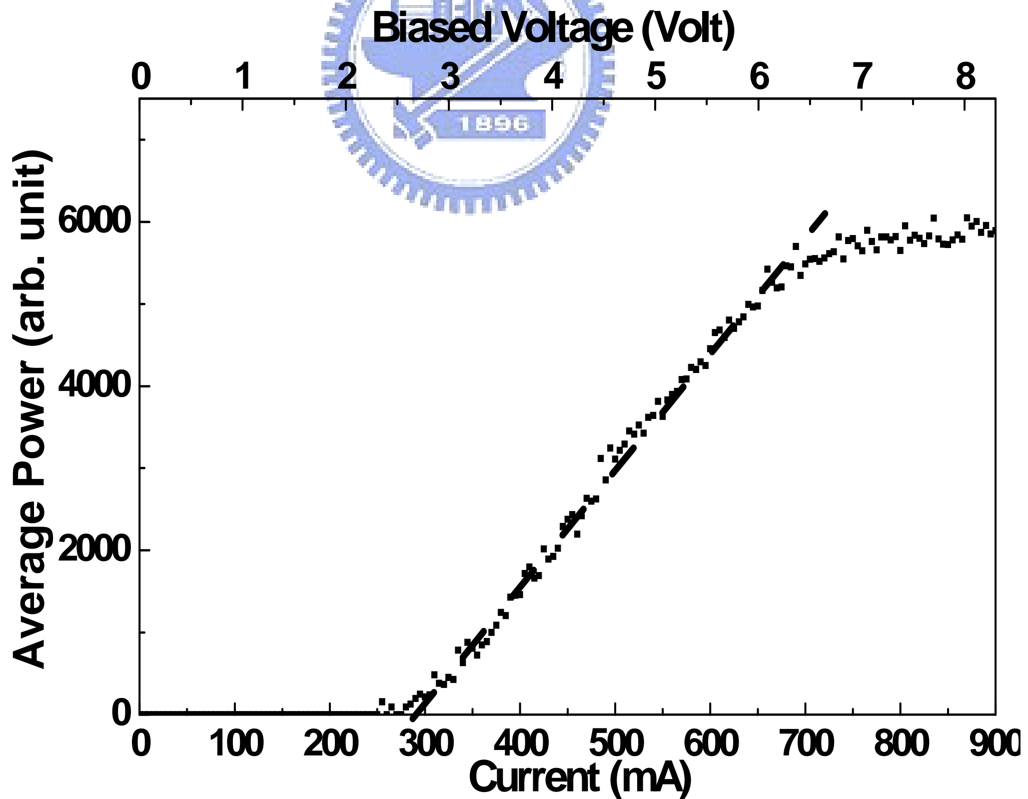

Fig. 10 The average EL power as a function of pulsed current and voltage. The inset figure shows CW (dashed line) and pulsed (dotted line) current-voltage responses of $Ag/SiO_2:Si^+/n$-Si/Ag MOS diode with $SiO_2:Si^+$ annealing at 1100°C for 3hrs.

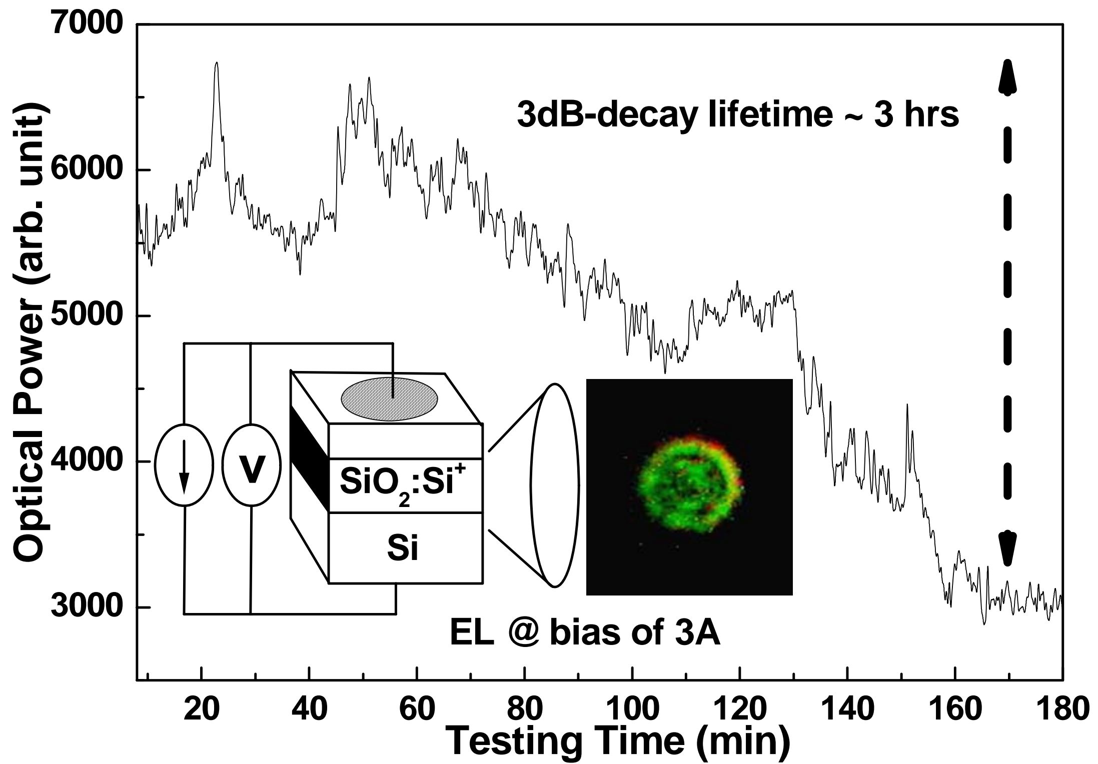

Fig. 11 Lifetime testing of Ag/SiO_2:Si^+/n-Si/Ag MOS diode under pulsed-current EL operation. The inset figure plots the operating condition of the MOS diode and its EL pattern at bias of 3 A.

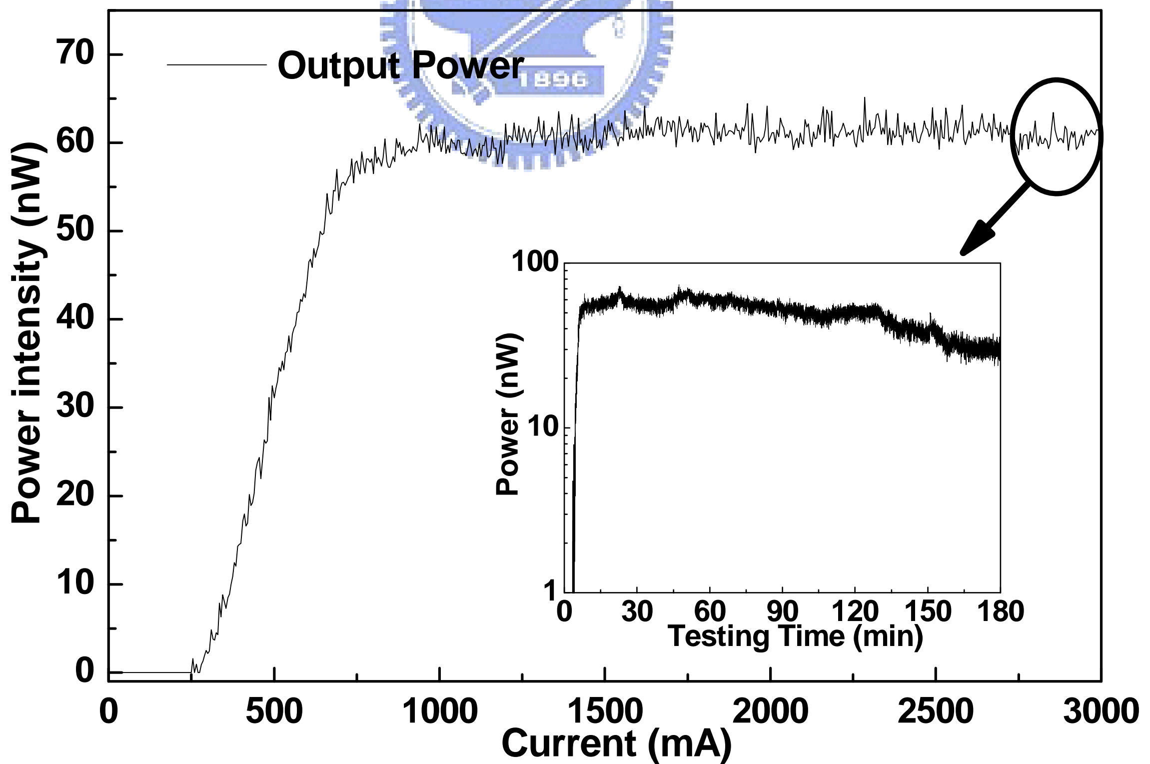

Fig. 12 Pulsed EL power as a function of the bias current. The inset figure is the lifetime and decaying rate of the Ag/SiO_2:Si^+/n-Si/Ag MOS diode under pulsed-current EL operation.

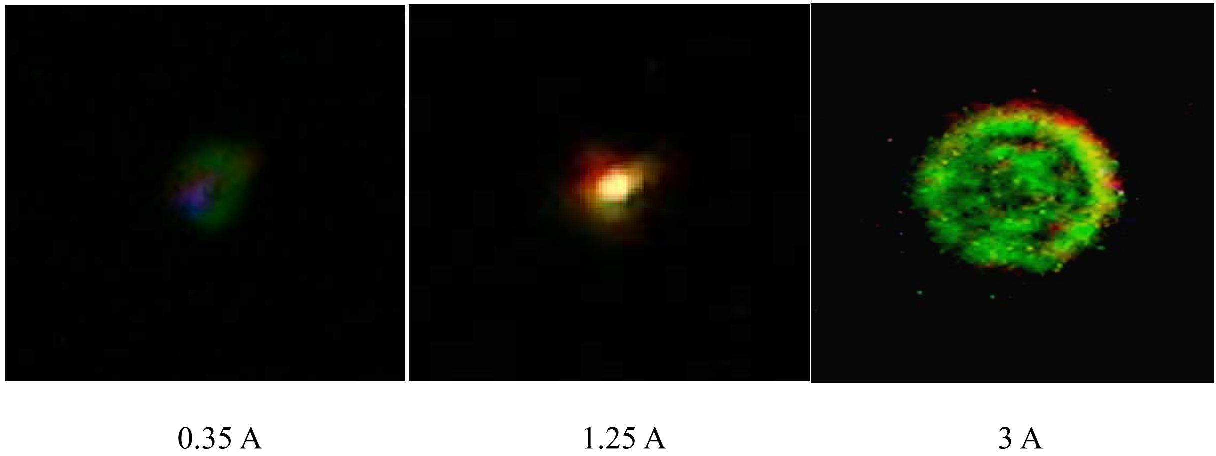

Fig. 13 EL patterns at different bias currents of 0.35 (left), 1.25 (middle) and 3 A (right).

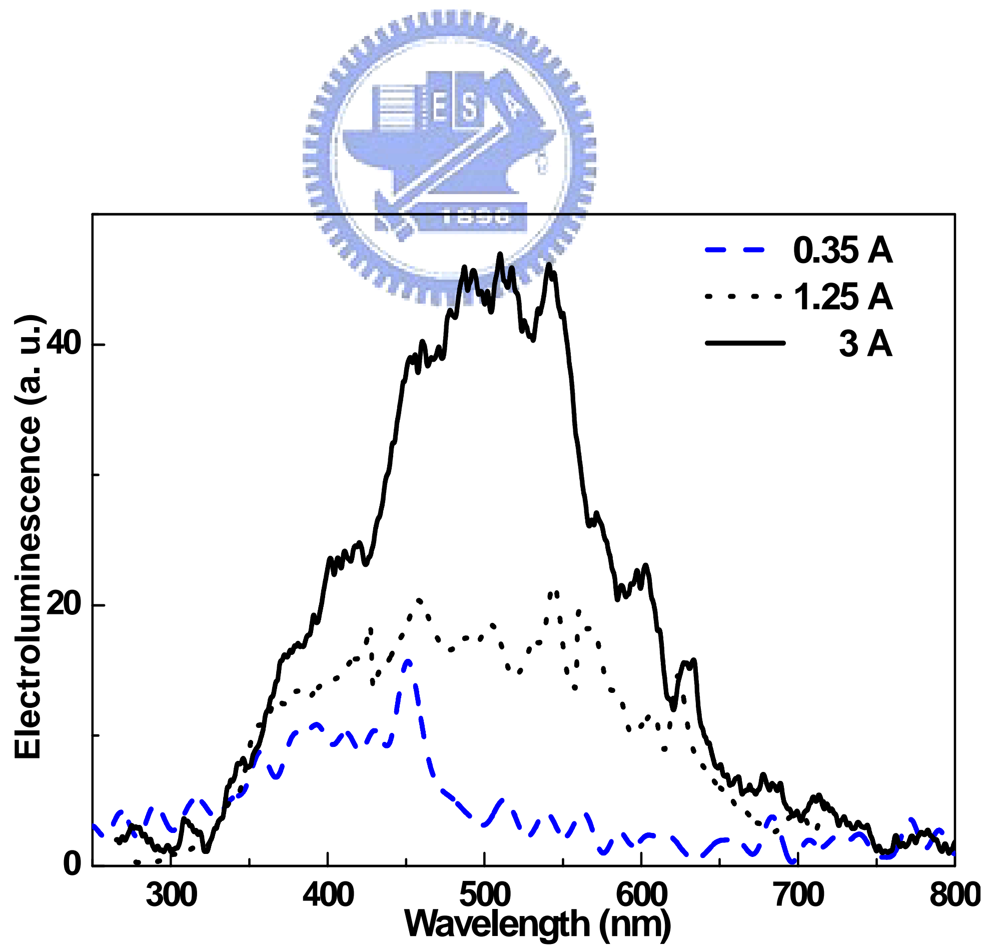

Fig. 14 EL spectra of the $Ag/SiO_2:Si^+/n\text{-}Si/Ag$ MOS diode at different bias currents of 0.35 A (dash line), 1.25 A (dot line) and 3 A (solid line).

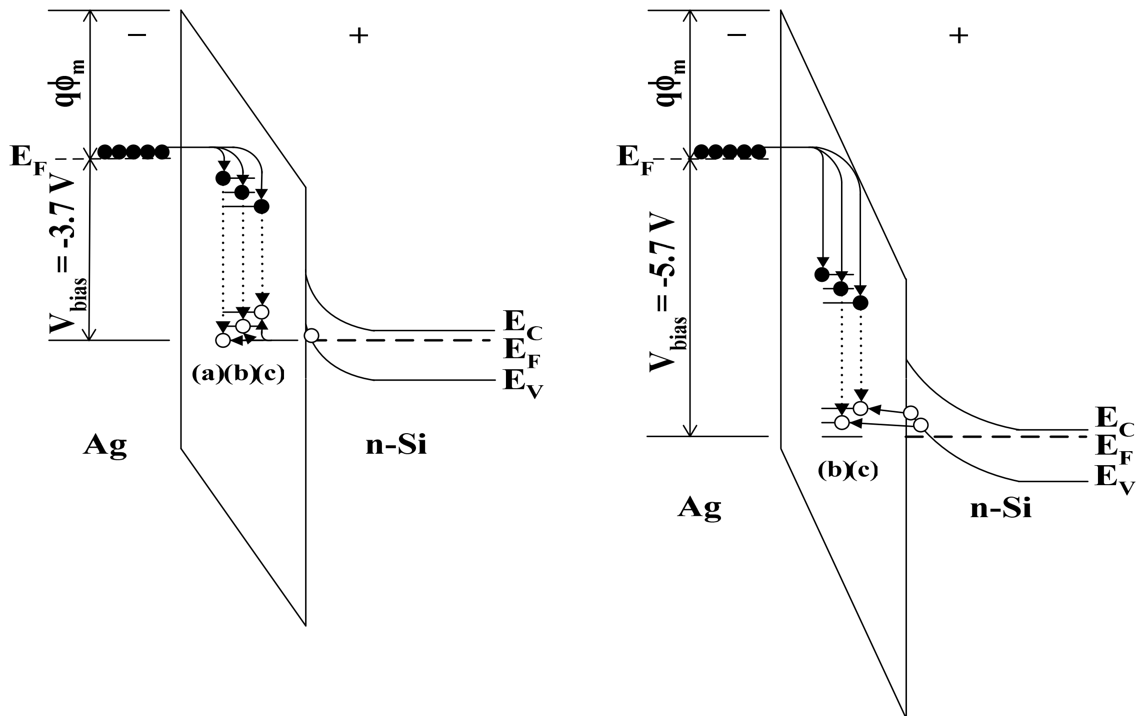

Fig. 15 Energy band diagrams of the Ag/SiO_2:Si^+/n-Si/Ag structure with metal-oxide barrier potential of ϕ_m = 3.28 V under reverse bias at 3.7 V (left part) and 5.7 V (right part). Three defect-related irradiative emissions at (a) 415 nm from the WOB defect, (b) 455 nm from the NOV defect and (c) 520 nm from the E'_δ defect.